PHYSICAL REVIEW B **89**, 161408(R) (2014)

Absence of the Aharonov-Bohm effect of chiral Majorana fermion edge states

Sunghun Park,[1] Joel E. Moore,[2,3] and H.-S. Sim[1,*]
[1]*Department of Physics, Korea Advanced Institute of Science and Technology, Daejeon 305-701, Korea*
[2]*Department of Physics, University of California, Berkeley, California 94720, USA*
[3]*Materials Sciences Division, Lawrence Berkeley National Laboratory, Berkeley, California 94720, USA*
(Received 26 July 2013; revised manuscript received 16 April 2014; published 25 April 2014)

Majorana fermions in a superconductor hybrid system are charge neutral zero-energy states. For the detection of this unique feature, we propose an interferometry of a chiral Majorana edge channel, formed along the interface between a superconductor and a topological insulator under an external magnetic field. The superconductor is of a ring shape and has a Josephson junction that allows the Majorana state to enclose continuously tunable magnetic flux. Zero-bias differential electron conductance between the Majorana state and a normal lead is found to be independent of the flux at zero temperature, manifesting the Majorana feature of a charge neutral zero-energy state. In contrast, the same setup on graphene has no Majorana state and shows Aharonov-Bohm effects.

DOI: 10.1103/PhysRevB.89.161408 PACS number(s): 71.10.Pm, 73.23.−b, 74.45.+c, 74.90.+n

Introduction. There have been efforts to find evidence of Majorana fermions in superconductor hybrid systems [1–4]. In the systems, Majorana fermions appear at zero excitation energy in the superconducting energy gap. Recent experiments [5–8] studied a superconductor coupled to a semiconductor nanowire with strong spin-orbit coupling. The result such as zero-bias resonant tunneling agrees with the behavior of a Majorana bound state [9,10] formed at the end of a topological superconducting region. Other experiments [11] found an anomalous Fraunhofer diffraction pattern in a Josephson junction on a topological insulator (TI) [12,13]. This may be related to a Majorana state [14], however, more studies are necessary to understand it. There are also other proposals [15–22], including Z_2 interferometers [15–17] formed along a superconductor-ferromagnet interface on a TI.

To achieve more direct evidence, one needs to explore other Majorana features. One goal of the present work is to develop an experimentally feasible test for a Majorana fermion as a *charge neutral* zero-energy state, based on an Aharonov-Bohm interferometer; a similar strategy was adapted [23] to experimentally confirm the charge neutrality of neutrons. As a charge neutral particle, Majorana fermions will not show Aharonov-Bohm effects. This is a direct consequence of the fact that Majorana fermions "are their own antiparticles," namely, that the Majorana operator is self-conjugate or real, not carrying a complex Aharonov-Bohm phase factor.

It is nontrivial to find an interferometry where Majorana states do not show Aharonov-Bohm effects, because of a few reasons. First, the interferometry has to be formed solely by extended Majorana channels [15–17]. When an interference loop enclosing magnetic flux is composed of Majorana bound states and electron paths, Aharonov-Bohm effects occur [24]. It is because a Majorana state in solids is a superposition of an electron and a hole, hence, the tunneling between a Majorana state and an electron path carries flux information. Second, the interferometry should enclose continuously tunable magnetic flux. Its candidate is a superconducting ring with a Josephson junction, rather than a closed ring [20] enclosing quantized flux. This setup was recently studied [18,19] in a different context from our study.

In this work, we propose a Majorana version of quantum Hall interferometers [25] for detecting a Majorana state (see Fig. 1). It is based on a chiral Majorana fermion edge channel, formed along the interface between an s-wave superconductor ring and the integer quantum Hall state of a TI surface. The ring has a Josephson junction, which connects the Majorana channels of the inner and outer boundaries of the ring. It allows the Majorana state to enclose continuously tunable magnetic flux Φ. Zero-bias electron tunneling differential conductance from a normal lead to the ring is found to be independent of Φ at zero temperature, demonstrating the unique Majorana feature of a charge neutral zero-energy state. The setup also exhibits Majorana features at finite bias and temperature. To prove that this behavior is a sensitive probe of Majorana physics, we show that in the same setup on graphene, which also has zero-energy states (because of Berry phase π of its Dirac fermions) but has Bogoliubov (a complex superposition of an electron and a hole, such as quasiparticles in a typical superconductor) rather than Majorana fermions, Aharonov-Bohm effects are present. We discuss the experimental feasibility of our setup.

Chiral Majorana edge channel. In Fig. 1, a magnetic field B is perpendicularly applied to the TI surface outside the proximity region with superconducting gap Δ_0. The resulting Landau-level orbits of the surface undergo Andreev reflections [26] and form chiral Majorana edge channels along the interface between the superconducting-gap region and the Landau-gap region [27,28]; a Majorana channel can be also formed when a Zeeman gap induced by a ferromagnet [15–17,21] replaces the Landau gap. The number of the channels is odd (since the TI has an odd number of Dirac cones), indicating that the Majorana states are stable, and it is determined by B, the chemical potential μ [27], and g factor g [28] of the TI surface. Hereafter we focus on the case of a single Majorana channel γ well localized near the interface, and on energy scales $\ll \Delta_0$. The particle-hole symmetry ensures that γ satisfies $\gamma(x) = \gamma^\dagger(x)$ and $\gamma_k^\dagger = \gamma_{-k} \sim \int dx\, \gamma(x) e^{-ikx}$, with coordinate x and momentum k along the channel. Its Hamiltonian is

$$H_{\rm MF} = -i\hbar v_M \int dx\, \gamma(x) \partial_x \gamma(x). \quad (1)$$

*hssim@kaist.ac.kr

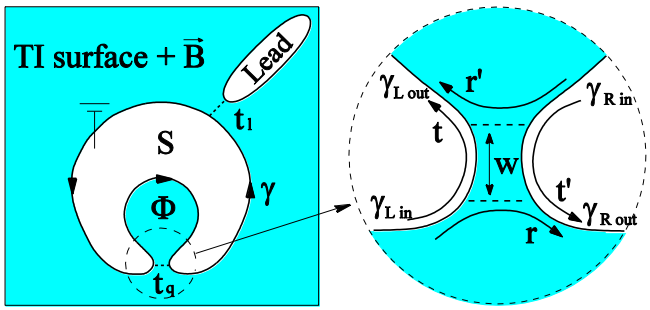

FIG. 1. (Color online) Interferometer of a chiral Majorana fermion edge channel γ (arrows), formed along the interface between an s-wave superconductor ring (S) and the integer quantum Hall state of a topological-insulator (TI) surface under a magnetic field $\vec{B}$. It has a Josephson junction (dashed circle, right panel), which behaves as a beam splitter for the Majorana channel and allows the channel to enclose continuously tunable magnetic flux Φ. Zero-bias electron tunneling differential conductance between a normal lead and the ring shows that the Majorana state is independent of Φ.

$v_M = v_M(B,\Delta_0,\mu,g)$ is the propagation velocity of γ.

The Josephson junction in Fig. 1 is in the short junction limit. It describes the coupling of Majorana channels $\gamma_{L,R}$ between its two sides. Its model Hamiltonian [14] is

$$H_{JJ} = -2i \int dx\, t_q(x)\gamma_L(x)\gamma_R(x). \tag{2}$$

$t_q(x) = \Delta_0 \cos(\phi/2)$ for $|x - x_0| \leqslant W/2$, and $t_q(x) = 0$ otherwise, where x_0 and W are the junction center and width. Superconducting phase difference ϕ across the junction is induced by Φ as $\phi/2 = 2\pi\Phi/\Phi_{0,e}$ with $\Phi_{0,e} = h/e$. The junction behaves as a beam splitter of γ_k. The channel $\gamma_{k,\text{in}}$ with momentum k, incoming to the junction from the outer or inner boundary of the ring, is scattered into outgoing ones, $\gamma_{k,\text{out}}$. We obtain the unitary scattering matrix S_{JJ} for this (see Fig. 1),

$$\begin{pmatrix}\gamma_{L,\text{out}}\\ \gamma_{R,\text{out}}\end{pmatrix} = S_{JJ}\begin{pmatrix}\gamma_{L,\text{in}}\\ \gamma_{R,\text{in}}\end{pmatrix}, \quad S_{JJ} = \begin{pmatrix}t & r'\\ r & t'\end{pmatrix}, \tag{3}$$

reflection coefficient $r = -r' = (\eta^{-1}\sinh\alpha)\Delta_0\cos\frac{\phi}{2}$, and transmission coefficient $t = t' = \hbar v_M\alpha/(\eta W)$, where $\alpha = W\sqrt{[\Delta_0/(\hbar v_M)]^2\cos^2(\phi/2) - k^2}$ and $\eta = \hbar v_M(\alpha W^{-1}\cosh\alpha - ik\sinh\alpha)$; the same expression was found in Ref. [19]. Note that r and t depend on ϕ, hence, on Φ in a nontrivial way; when $\phi = \pi$ and $k \to 0$, Majorana states occur in the junction so that $r \to 0$ and $t \to 1$. We will see that the flux dependence does not affect the Majorana resonance state at $k = 0$ in our setup.

Resonance. We study scattering between the incoming and outgoing channels of the outer ring boundary, $\gamma_{L,\text{in}}$ and $\gamma_{R,\text{out}}$, at the Josephson junction. Because there is no loss of Majorana fermions along the inner boundary of the ring, the scattering causes phase shift θ_Λ only. From Eq. (3) and $\gamma_{R,\text{in}} = e^{ikd}\gamma_{L,\text{out}}$ (the accumulation of dynamical phase kd along the circumference d of the inner ring boundary), we obtain $\gamma_{R,\text{out}} = e^{i\theta_\Lambda}\gamma_{L,\text{in}}$,

$$e^{i\theta_\Lambda} = r + \frac{tt'e^{ikd}}{1 - r'e^{ikd}} = \frac{r + (r^2+t^2)e^{ikd}}{1 + re^{ikd}} \tag{4}$$

for $|r| \neq 1$. The first equality of Eq. (4) comes from the direct scattering between $\gamma_{L,\text{in}}$ and $\gamma_{R,\text{out}}$ and from the paths with multiple winding of the flux Φ along the inner boundary, while the second comes from the unitarity of S_{JJ}.

We notice a number of interesting points from Eq. (4). First, θ_Λ depends on Φ in a nontrivial way through $r(\Phi)$ and $t(\Phi)$. This is distinct from usual electron cases where the flux dependence couples with dynamical phase such as $kd + 2\pi\Phi/\Phi_{0,e}$. Second, at zero energy (i.e., $k = 0$), the following are satisfied, irrespective of Φ: $r_0(\Phi) \equiv r(k=0) = \tanh(\frac{W\Delta_0}{\hbar v_M}\cos\frac{2\pi\Phi}{\Phi_{0,e}})$ is real, $r^2 + t^2 = 1$ (partially from the unitarity of S_{JJ}), thus $e^{i\theta_\Lambda} = 1$ is real. These are attributed to the fact that the Majorana operator is real self-conjugate. Third, near zero energy ($k \simeq 0$), $r^2 + t^2 \simeq 1$ and $r \simeq |r_0(\Phi)|\text{sgn}(\cos 2\pi\Phi/\Phi_{0,e})$ are almost real [29]. Then, when $kd = m\pi$ with $m = 1,2,\ldots$ is satisfied, the phase shift becomes $\theta_\Lambda \simeq m\pi$, almost independent of Φ. Considering the resonance condition $kd + \pi + \arg r = 2m'\pi$ (with integer m') of the inner boundary and $\arg r = \pi[1 - \text{sgn}(\cos 2\pi\Phi/\Phi_{0,e})]/2$, we find that $kd = m\pi$ means on or off resonance of the inner boundary, depending on Φ. However, regardless of on or off resonance, θ_Λ is almost independent of Φ. In contrast, for $kd \neq m\pi$, θ_Λ varies with Φ. Fourth, Eq. (4) describes well the vortex limit where the ring is fully closed. In this case, Φ will be quantized as $\Phi = l\Phi_{0,e}/2$ with integer l so that $r = (-1)^l$ and $t = 0$; hence, $e^{i\theta_\Lambda} = (-1)^l$.

The resonance condition of the whole setup (including both the inner and outer boundaries) is found as

$$kL + \pi + n_v\pi + \theta_\Lambda = 2n\pi, \tag{5}$$

where kL is the dynamical phase along the circumference L of the outer boundary, π is the Berry phase [15–17] of Majorana fermions circulating the setup, n_v is the number of vortices inside the superconducting area, and n is an integer.

The resonances can be detected by electron tunneling from a normal lead to the outer ring boundary. The lead is modeled by one-dimensional electrons with Hamiltonian $H_L = -i\hbar v_L\sum_{\sigma=\uparrow,\downarrow}\int_{-\infty}^{\infty} dy\,\psi_\sigma^\dagger(y)\partial_y\psi_\sigma(y)$, where $\psi_\sigma^\dagger(y)$ is the electron field operator with spin σ at position y and v_L is electron velocity in the lead. The tunneling Hamiltonian is $H_{\text{MF}-L} = -2it_l\gamma(x_1)\bar{\gamma}(y_1)$, where tunneling strength t_l is real, x_1 and y_1 are tunneling positions, $\bar{\gamma}(y_1) = (1/2)\sum_\sigma[e^{i\chi_\sigma}\psi_\sigma^\dagger(y_1) + e^{-i\chi_\sigma}\psi_\sigma(y_1)]$ is a Majorana representation of states in the lead, and $e^{i\chi_\sigma}$ is the phase factor from the tunneling. At zero temperature, the differential conductance dI/dV from the lead with bias V to the grounded ring has the form [17] of

$$\frac{dI}{dV} = \frac{2e^2}{h}|s_{he}|^2 = \frac{2e^2}{h}\frac{\tilde{t}_l^4\cos^2(\theta_s/2)}{\sin^2(\theta_s/2) + \tilde{t}_l^4\cos^2(\theta_s/2)}, \tag{6}$$

where s_{he} describes Andreev reflections in the lead, $\tilde{t}_l = t_l/(2\hbar\sqrt{v_M v_L})$, and $\theta_s = kL + \pi + n_v\pi + \theta_\Lambda$. The resonance condition in Eq. (5) is written as $\theta_s = 2n\pi$.

We first discuss dI/dV at zero temperature (see Fig. 2). At zero bias, it is determined by the Majorana state with $k = 0$, which shows $e^{i\theta_\Lambda} = 1$. Hence, the resonance condition of Eq. (5) and $dI/dV(V = 0)$ do not depend on Φ. This demonstrates the absence of Aharonov-Bohm effects of the Majorana state, the manifestation of the fact that Majorana fermions are charge neutral. $dI/dV(V = 0)$ is also independent of system

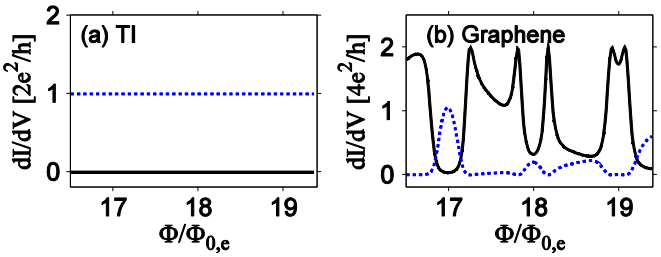

FIG. 2. (Color online) (a) dI/dV of the setup on a TI surface (see Fig. 1) at zero temperature and at zero bias, as a function of the magnetic flux Φ, for the cases of odd n_v (blue dashed curve) and even n_v (black solid). (b) The same as in (a), but for the setup on graphene. Both in (a) and (b), B changes from 0.85 T to 1 T, and we choose $\Delta_0 = 1.5$ meV, $L = 7000$ nm, $d = 1000$ nm, g factor $g = 2$, chemical potential $\mu = 15$ meV, and Fermi velocity $v_f = 5 \times 10^5$ m/s; these parameters lead to $v_M = 0.14 v_f$. We also choose W such that the maximum value of $|r|^2$ is 0.6 for (a) and 0.8 for (b), and $\tilde{t}_l = 0.48$ for (a) and $\tilde{t}_l = 0.62$ for (b). The Majorana state in case (a) does not exhibit Aharonov-Bohm effects, while the zero-energy Bogoliubov excitations in graphene case (b) do.

lengths (L, d, and W) and coupling strengths (t_q and t_l). It shows the Z_2 property [15–17] that the interferometry has off (on) resonance and $dI/dV = 0$ ($dI/dV = 2e^2/h$), when n_v is even (odd).

Next, we discuss dI/dV at zero temperature, but at finite bias (see Fig. 3). The zero-bias behavior mentioned above appears at $V = 0$. At finite bias, resonances occur whenever Eq. (5) is satisfied. For low energy of $kd \ll 1$, we find $\theta_\Lambda \simeq \frac{1-r_0}{1+r_0} kd$ and obtain resonance center V_r,

$$eV_r \simeq \frac{\hbar v_M (2n\pi - \pi - n_v \pi)}{L + d(1-r_0)/(1+r_0)}. \tag{7}$$

V_r depends on Φ through $(1-r_0)/(1+r_0)$, oscillating with period $\Phi_{0,e}$. $|V_r|$ has maxima (minima) at (half-)integer multiples of $\Phi_{0,e}$; the gradual decrease of $|V_r|$ with increasing Φ is due to the dependence of v_M on B. For $kd \ll 1$, the level broadening ΔV of the resonances also depends on Φ as

$$e\Delta V \simeq \frac{2\hbar v_M \tilde{t}_l^2}{L + d(1-r_0)/(1+r_0)}, \tag{8}$$

which has maxima (minima) at (half-)integer multiples of $\Phi_{0,e}$. This behavior of V_r and ΔV is the consequence of the Majorana feature of $t_q \propto \cos(\phi/2)$ in Eq. (2). Note that the range of V in Fig. 3 does not reach the condition of $kd = m\pi$ with nonzero m, at which $\theta_\Lambda \simeq m\pi$ and dI/dV is almost independent of Φ (as discussed above). We emphasize that

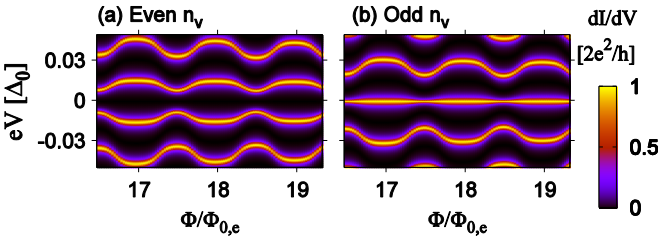

FIG. 3. (Color online) dI/dV of the setup on a TI surface at zero temperature, as a function of Φ and V, for the case of (a) even n_v and (b) odd n_v. The same parameters as in Fig. 2 are used.

at $V = 0$ and zero temperature, dI/dV remains constant (0 or $2e^2/h$) for finite $\Delta V(\Phi)$ [even if $\Delta V(\Phi)$ is larger than resonance level spacing] for both even and odd n_v.

At finite temperature T, one has $dI/dV\ (V=0) = \frac{2e^2}{h} \int_0^\infty d\varepsilon |s_{he}(\varepsilon)|^2 \frac{\beta}{1+\cosh \beta\varepsilon}$ [15], where $\beta = (k_B T)^{-1}$ and $\varepsilon = \hbar v_M k$ is the excitation energy. In this case, thermal broadening causes $dI/dV\ (V=0)$ to depend on Φ. From $|s_{he}|$ in Eq. (6), we find that at $k_B T \ll e\Delta V$ and $\hbar v_M/L$, $dI/dV\ (V=0)$ weakly depends on Φ as $dI/dV\ (V=0) = \frac{2e^2}{h}[1 - \frac{4(k_B T)^2}{(e\Delta V)^2} + O(T^4)]$ for odd n_v, and as $dI/dV\ (V=0) \simeq \frac{2e^2}{h} \frac{4\tilde{t}^8 (k_B T)^2}{(e\Delta V)^2}$ for even n_v. The dependence on Φ becomes suppressed as $\sim T^2$ at lower temperature, in sharp contrast to the usual electron interferometers [25] where interference visibility becomes enhanced at lower temperature. This is a finite-temperature signature of the absence of Aharonov-Bohm effects of the Majorana state. Note that n_v can vary by temperature or B change, leading to jumps of $dI/dV\ (V=0)$ between 0 and $2e^2/h$ [30,31]. The jumps are distinct from Aharonov-Bohm effects as they are not periodic in Φ.

Non-Majorana case. To compare the above findings with a non-Majorana case, we consider the same setup on graphene. Similarly to a TI, graphene has Dirac fermions [32], and zero-energy excitations by superconducting proximity effects. But it has two Dirac cones at K and K' valleys, which are transformed into each other by time reversal. Moreover, the momentum of its Dirac fermions couples to the pseudospin representing the sublattice sites, rather than spin. As a result, near zero excitation energy, there occur four chiral edge channels of $\Psi_1 = (e^K_\uparrow, h^{K'}_\downarrow)$, $\Psi_2 = (e^{K'}_\uparrow, h^K_\downarrow)$, $\Psi_3 = (e^K_\downarrow, h^{K'}_\uparrow)$, and $\Psi_4 = (e^{K'}_\downarrow, h^K_\uparrow)$ along the interface between the superconducting region and the Landau-gap region [26], where Ψ represents an electron-hole (e-h) pair with opposite spin ($\uparrow$, $\downarrow$) and valley. In the same way as the TI case, we compute dI/dV, taking into account the energy dispersion of Ψ_i [33]. We ignore intervalley mixing and spin scattering in the setup, and neglect minor correction to S_{JJ} by Zeeman energy for simplicity; these effects do not alter our finding that dI/dV shows Aharonov-Bohm effects at $V = 0$ in graphene.

The chiral channels in graphene were theoretically studied in Ref. [26], ignoring Zeeman energy. We derive the energy dispersion $\epsilon_i(k) = \hbar v_D k + E_{Z,i}$ of channel $\Psi_{i=1,2,3,4}$, following Ref. [26], but including Zeeman energy. v_D is the propagation velocity, and the Zeeman contribution $E_{Z,i}$ is finite and channel dependent [28,33]. For zero Zeeman energy,

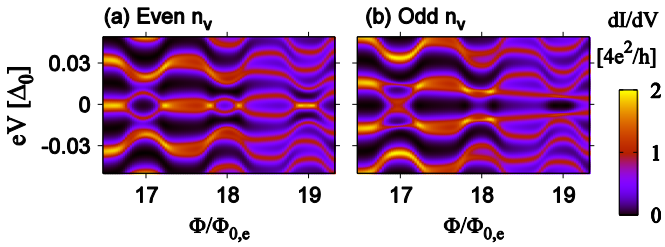

FIG. 4. (Color online) dI/dV of the setup on graphene at zero temperature, as a function of Φ and V, for the case of (a) even n_v and (b) odd n_v. The same parameters as in Fig. 2 are used. The result is distinct from Fig. 3, since there are four chiral channels, each carrying nonzero charge, in the graphene case.

Ψ_i is charge neutral with equal weight between its electron and hole parts, and dI/dV can be independent of Φ at $V = 0$. In contrast, in the realistic case of finite Zeeman energy, Ψ_i carries charge even at zero energy, since its electron and hole parts have opposite spin to each other, and hence, have different weight due to Zeeman energy. As a result, Ψ_i does not satisfy the Majorana condition of $\gamma_k^\dagger = \gamma_{-k}$ and $\gamma^\dagger(x) = \gamma(x)$, and $dI/dV(V = 0)$ exhibits Φ-dependent oscillation for both even and odd n_v [see Figs. 2(b) and 4].

Conclusion. The absence of Aharonov-Bohm effects at zero bias in our Majorana interferometry is a direct consequence of the essence that a Majorana fermion is its own antiparticle, i.e., a real operator. It is in contrast to the Φ dependence of dI/dV of the same setup at large bias. It should be also distinguished from Bogoliubov fermions, such as those in the graphene case, that show Aharonov-Bohm effects unless there is fine-tuning (e.g., unrealistic tuning to zero Zeeman energy for graphene).

We now discuss experimental feasibility. For the superconducting ring, one may use niobium. It has $\Delta_0 \approx 1.5$ meV, superconducting critical temperature of 9 K, the lower and upper critical fields of 2.7 and 4 T, coherence length $\xi_C \simeq 200$ nm, and penetration depth $\xi_D \simeq 350$ nm [34–36]. It was used to study proximity effects under high magnetic fields in graphene [34] and in a two-dimensional electron gas [37,38]. While $d/(2\pi)$ should be longer than magnetic length ($\simeq$25 nm at $B = 1$ T), L needs to satisfy $\pi\xi_C, \pi\xi_D < L < \hbar v_M/(k_B T)$, which means 350 nm $< L/\pi <$ 11 500 nm at $T = 12$ mK; Majorana resonance energies are resolved in the setup with $L < \hbar v_M/(k_B T)$, we estimate $v_M \simeq 0.14 v_f$ [27], and $T \simeq 12$ mK was achieved [11]. This indicates that a range of L is available for our prediction. Under the parameters ($L =$ 7000 nm) used in Fig. 2, the energy splitting near zero bias is about 0.024 meV in the Majorana case (see Fig. 3), and 0.022 meV in the graphene case (Fig. 4). Hence, the two cases are distinguishable at a currently available temperature of 12 mK ($\simeq$0.001 meV).

Acknowledgments. We thank D. Goldharber-Gordon for useful discussions. We acknowledge support by Korea NRF (Grant No. 2012S1A2A1A01030312; H.-S.S.) and DARPA (J.E.M).

[1] A. Kitaev, Phys. Usp. **44**, 131 (2001).
[2] M. Z. Hasan and C. L. Kane, Rev. Mod. Phys. **82**, 3045 (2010).
[3] J. Alicea, Rep. Prog. Phys. **75**, 076501 (2012).
[4] M. Leijnse and K. Flensberg, Semicond. Sci. Technol. **27**, 124003 (2012).
[5] V. Mourik, K. Zuo, S. M. Frolov, S. R. Plissard, E. P. A. M. Bakkers, and L. P. Kouwenhoven, Science **336**, 1003 (2012).
[6] A. Das, Y. Ronen, Y. Most, Y. Oreg, M. Heiblum, and H. Shtrikman, Nat. Phys. **8**, 887 (2012).
[7] M. T. Deng, C. L. Yu, G. Y. Huang, M. Larsson, P. Caroff, and H. Q. Xu, Nano Lett. **12**, 6414 (2012).
[8] L. P. Rokhinson, X. Liu, and J. K. Furdyna, Nat. Phys. **8**, 795 (2012).
[9] Y. Oreg, G. Refael, and F. von Oppen, Phys. Rev. Lett. **105**, 177002 (2010).
[10] R. M. Lutchyn, J. D. Sau, and S. Das Sarma, Phys. Rev. Lett. **105**, 077001 (2010).
[11] J. R. Williams, A. J. Bestwick, P. Gallagher, S. S. Hong, Y. Cui, A. S. Bleich, J. G. Analytis, I. R. Fisher, and D. Goldhaber-Gordon, Phys. Rev. Lett. **109**, 056803 (2012).
[12] B. Sacépé, J. B. Oostinga, J. Li, A. Ubaldini, N. J. G. Couto, E. Giannini, and A. F. Morpurgo, Nat. Commun. **2**, 575 (2011).
[13] M. Veldhorst, M. Snelder, M. Hoek, T. Gang, V. K. Guduru, X. L. Wang, U. Zeitler, W. G. van der Wiel, A. A. Golubov, H. Hilgenkamp, and A. Brinkman, Nat. Mater. **11**, 417 (2012).
[14] L. Fu and C. L. Kane, Phys. Rev. Lett. **100**, 096407 (2008).
[15] L. Fu and C. L. Kane, Phys. Rev. Lett. **102**, 216403 (2009).
[16] A. R. Akhmerov, J. Nilsson, and C. W. J. Beenakker, Phys. Rev. Lett. **102**, 216404 (2009).
[17] K. T. Law, P. A. Lee, and T. K. Ng, Phys. Rev. Lett. **103**, 237001 (2009).
[18] M. Diez, I. C. Fulga, D. I. Pikulin, M. Wimmer, A. R. Akhmerov, and C. W. J. Beenakker, Phys. Rev. B **87**, 125406 (2013).
[19] B. J. Wieder, F. Zhang, and C. L. Kane, Phys. Rev. B **89**, 075106 (2014).
[20] B. Beri, Phys. Rev. B **85**, 140501(R) (2012).
[21] Y. Tanaka, T. Yokoyama, and N. Nagaosa, Phys. Rev. Lett. **103**, 107002 (2009).
[22] J. Li, G. Fleury, and M. Büttiker, Phys. Rev. B **85**, 125440 (2012).
[23] D. M. Greenberger, D. K. Atwood, J. Arthur, C. G. Shull, and M. Schlenker, Phys. Rev. Lett. **47**, 751 (1981).
[24] L. Fu, Phys. Rev. Lett. **104**, 056402 (2010).
[25] Y. Ji, Y. Chung, D. Sprinzak, M. Heiblum, D. Mahalu, and H. Shtrikman, Nature (London) **422**, 415 (2003).
[26] A. R. Akhmerov and C. W. J. Beenakker, Phys. Rev. Lett. **98**, 157003 (2007).
[27] R. P. Tiwari, U. Zülicke, and C. Bruder, Phys. Rev. Lett. **110**, 186805 (2013).
[28] S. Park and H.-S. Sim (unpublished).
[29] For $\hbar v_M k \ll \Delta_0$, $r \simeq r_0[1 + i\frac{r_0 k W_\Delta}{\cos(2\pi\Phi/\Phi_{0,e})}]$ and $r^2 + t^2 \simeq 1 + i\frac{2r_0 k W_\Delta}{\cos(2\pi\Phi/\Phi_{0,e})}$, where $W_\Delta \equiv \hbar v_M/\Delta_0$.
[30] A. L. Rakhmanov, A. V. Rozhkov, and Franco Nori, Phys. Rev. B **84**, 075141 (2011).
[31] P. A. Ioselevich, P. M. Ostrovsky, and M. V. Feigel'man, Phys. Rev. B **86**, 035441 (2012); P. A. Ioselevich and M. V. Feigel'man, New J. Phys. **15**, 055011 (2013).
[32] A. H. Castro Neto, F. Guinea, N. M. R. Peres, K. S. Novoselov, and A. K. Geim, Rev. Mod. Phys. **81**, 109 (2009).
[33] See Supplemental Material at http://link.aps.org/supplemental/10.1103/PhysRevB.89.161408 for the details.
[34] P. Rickhaus, M. Weiss, L. Marot, and C. Schönenberger, Nano Lett. **12**, 1942 (2012).
[35] A. F. Morpurgo, J. Kong, C. M. Marcus, and H. Dai, Science **286**, 263 (1999).
[36] J. B. Oostinga, L. Maier, P. Schüffelgen, D. Knott, C. Ames, C. Brüne, G. Tkachov, H. Buhmann, and L. W. Molenkamp, Phys. Rev. X **3**, 021007 (2013).
[37] J. Eroms, D. Weiss, J. De Boeck, G. Borghs, and U. Zülicke, Phys. Rev. Lett. **95**, 107001 (2005).
[38] D. Uhlisch, S. G. Lachenmann, Th. Schäpers, A. I. Braginski, H. Lüth, J. Appenzeller, A. A. Golubov, and A. V. Ustinov, Phys. Rev. B **61**, 12463 (2000).